

VIP

# Bridged Aromatic Oxo- and Thioethers with Intense Emission in Solution and the Solid State

Steffen Riebe<sup>+, [a]</sup>, Suliman Adam<sup>+, [c]</sup>, Bibhisan Roy,<sup>[a]</sup> Iván Maisuls,<sup>[b]</sup> Constantin G. Daniliuc,<sup>[d]</sup> Justin Dubbert,<sup>[a]</sup> Cristian A. Strassert,<sup>[b]</sup> Igor Schapiro,<sup>\*, [c]</sup> and Jens Voskuhl<sup>\*, [a]</sup>

**Abstract:** In this contribution, we report on a class of emitters based on bridged oxo- and/or thioethers revealing striking photoluminescence properties in fluid solution and in the solid state. In total, nine compounds were investigated concerning their photophysical properties, which were interpreted by quantum chemical calculations. To our delight, we discovered compounds possessing nearly identical photo-

luminescence quantum yields ( $\Phi_F$ ) in solution and in the solid state, which has been rarely reported so far. Besides these efforts, we shed light on the influence of polymorphism and solvent polarity on the emission properties. In addition, an in-depth X-ray diffractometric analysis was conducted to correlate molecular packing in the crystal with differences in the photophysical properties.

## Introduction

Traditional planar organic fluorophores (such as fluorescein or rhodamine) are generally luminescent in solution but non-emissive in the solid state, due to a phenomenon called aggregation-caused quenching (ACQ).<sup>[1]</sup> This occurs mainly because of strong  $\pi \cdots \pi$  stacking interactions leading to non-radiative decay. On the other hand, non-planar, flexible aromatic organic molecules are known to be non-emissive in solution, but highly emissive in the aggregated or solid state as well as in viscous media or when entrapped in a sterically demanding environment.<sup>[2]</sup> This effect is well-known since decades<sup>[3]</sup> and has been used e.g. for bio-imaging such as staining of double stranded DNA or RNA using thiazole orange<sup>[4]</sup>. This phenomenon was coined as aggregation-induced emission (AIE) around 20 years ago.<sup>[5]</sup> It is noteworthy, that this

term is slightly misleading since not only aggregation but also rigidification (e.g. by binding to a target or increasing the viscosity) of the emitters is needed to induce emission.<sup>[6]</sup> Hence, fluorophores generally fall into the category of non-emissive ACQ molecules or non-planar emissive AIE probes.<sup>[7]</sup> In between these groups (ACQ and AIE probes), there are emitters known, that show efficient emission both in solution and in the solid state. This class of compounds is typically described as “dual-state emitters” (DSE), which is somewhat confusing, since it leads to the assumption that emission occurs from different electronic states. Hence, to avoid confusion, we herein prefer calling them “solution and solid state emitters” (SSSE), implying emission based on the degree of aggregation.<sup>[8]</sup> To the best of our knowledge, only a small number of molecules, which show comparable emission intensities in the solid- and the solution-state are known. In 2015 *Tang* and co-workers reported triphenylamines featuring different phenyl-rotors able to exhibit comparable emission efficiencies in solution and the solid state, which was attributed to an effect claimed as conjugation induced rigidity (CIR), rigidifying the molecular conformation in solution and the phenyl-rotors suppress unfavored packing in the solid state.<sup>[9]</sup> More recently, the same group reported a series of solution- and solid- state emissive *p*-bis(2,2-dicyanovinyl)benzene derivatives, that showed solution and solid-state photoluminescence quantum yields  $\Phi_F$  of  $\sim 11.9\%$  and  $13.3\%$  respectively.<sup>[10]</sup>

In another attempt, *Goel* and co-workers found 17 SSSE emitters in a library composed of 108 compounds. However, their screened compounds were poorly emissive in the solid state ( $\Phi_F \sim 0.52\%$ ) although they showed high  $\Phi_F$  in solution ( $\sim 30\%$ ).<sup>[11]</sup> In continuation of such efforts, *Ling* and co-workers developed some solution and solid-state emitters using 3/2-substituted benzothiophene or benzofuranes.<sup>[12]</sup>

In a recent contribution, *Wan* and co-workers described imidazo[5,4-*b*]thieno[3,2-*e*]pyridines as versatile SSSE molecules exhibiting striking emission properties in solution and the solid state based on excited state intramolecular proton transfer (ESIPT) enhancement, which restricts twisted intramolecular

[a] S. Riebe,<sup>+</sup> Dr. B. Roy, J. Dubbert, Prof. Dr. J. Voskuhl  
Faculty of Chemistry (Organic Chemistry) and CENIDE  
University of Duisburg-Essen  
Universitätsstrasse 7, 45117 Essen (Germany)  
E-mail: jens.voskuhl@uni-due.de

[b] Dr. I. Maisuls, Prof. Dr. C. A. Strassert  
Institut für Anorganische und Analytische Chemie, CeNTech, CiMIC, SoN  
Westfälische Wilhelms-Universität Münster  
Heisenbergstraße 11, 48149 Münster (Germany)

[c] Dr. S. Adam,<sup>+</sup> Prof. Dr. I. Schapiro  
Fritz Haber Center for Molecular Dynamics Research, Institute of Chemistry  
The Hebrew University of Jerusalem  
9190401, Jerusalem (Israel)  
E-mail: Igor.Schapiro@mail.huji.ac.il

[d] Dr. C. G. Daniliuc  
Organisch-Chemisches Institut  
Westfälische Wilhelms-Universität  
Corrensstraße 40, 48149 Münster (Germany)

[\*] These authors contributed equally

Supporting information for this article is available on the WWW under <https://doi.org/10.1002/asia.202100492>

© 2021 The Authors. Chemistry - An Asian Journal published by Wiley-VCH GmbH. This is an open access article under the terms of the Creative Commons Attribution Non-Commercial License, which permits use, distribution and reproduction in any medium, provided the original work is properly cited and is not used for commercial purposes.

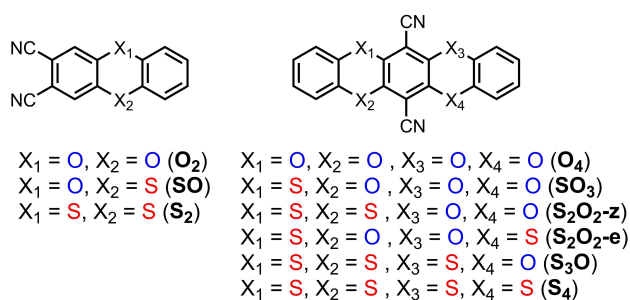
charge transfer (TICT). These compounds showed up to 53% quantum yield as solid and up to 92% in solution.<sup>[13]</sup> When arch-bridge-like thiazolo[5,4-*b*]thieno[3,2-*e*]pyridines were used, also SSSE properties were discovered utilizing additional hydrogen bonding to rigidify the rotors motion.<sup>[14]</sup> The same group extended their scope in 2021 to furo[2,3-*b*]furanes featuring quantum yields of up to 92% in solution and 42% in the solid state with emission in the blue-green portion of the electromagnetic spectrum.<sup>[15]</sup>

From the literature survey, it is clear that there is still a lack of suitable design strategies for efficient emitters in solution and the solid state with high emission efficiencies. In this contribution, we are presenting a class of compounds building the bridge between AIE and ACQ luminophores based on bridged oxo- and/or thioethers. These new luminophores are neither planar like ACQ probes nor are they rotor-based AIE-type probes. Their non-planarity was introduced by bridged heteroatoms, leading to a molecular twisting.<sup>[16]</sup> Hence, these SSSE luminophores will lead to a broader range of applications, due to their efficient emission both in the solid state and in fluid solution. To achieve such simultaneous emission from solution and in the solid state, substantial rigidity with limited intramolecular motions and a loss of planarity in their solid state (to prevent  $\pi \cdots \pi$  interactions leading to non-radiative decay) is simultaneously required. Hence, we reason that bridged oxo- and/or thioethers may provide a suitable platform to achieve these requirements while being able to overcome classic drawbacks of ACQ emitters (Scheme 1).

## Results and Discussion

In this study, two different classes of compounds with alternating positions of oxygen and sulphur heteroatoms were synthesized (Scheme 1). The detailed syntheses and full characterization of each compound is provided in the supporting information.

The syntheses started either by using 1,2-dichloro-phthalonitrile (compound  $O_2$ <sup>[17]</sup>,  $SO$ ,  $S_2$ ) or tetrachloro-terephthalonitrile (compound,  $O_4$ <sup>[18]</sup> and  $S_4$ ) followed by reaction with catechol, 1,2-benzendithiol or 2-hydroxythiophenol under basic conditions. For compounds  $SO_3$ ,  $S_2O_2-z$ ,  $S_2O_2-e$  and  $S_3O$ , first the mono-substituted compounds (A–C, see ESI) were synthesized



**Scheme 1.** Molecular structures of the target compounds investigated in this contribution.

starting from tetrachloro-terephthalonitrile, and finally coupled with 1,2-benzendithiol or 2-hydroxythiophenol under basic conditions yielding the desired compounds (Scheme 1 and ESI, Section 1 and Figures S1–S16).

Interestingly, we were able to isolate only one of the regioisomers (antiparallel) of compound  $S_2O_2-e$  using tetrachloro-terephthalonitrile as a precursor, whereas *Feng* and co-workers very recently isolated exclusively the parallel isomer of  $S_2O_2-e$  employing tetrafluoroterephthalonitrile as the starting material, which we were unable to isolate in significant amounts.<sup>[19]</sup>

To get a full understanding of the photophysical properties of the luminophores, steady state emission spectra as well as time-resolved photoluminescence decays ( $\tau$ ) in solution and the solid state were measured. Compounds ( $O_2$ )<sup>[17]</sup> and ( $O_4$ )<sup>[18]</sup> have been reported previously together with partial characterisation of the photophysical properties. However, we herein performed a systematic comparison of the luminophores by stepwise variation of the sulphur and oxygen content to check for the influence of electronegativity, size of the heteroatom and changes in the compounds' geometry. Considering the optical properties of  $O_2$ ,  $SO$  and  $S_2$  firstly, the absorption and excitation spectra of compound  $O_2$  ( $X_1$  and  $X_2 = \text{oxygen}$ ) in DMF exhibited a single band at 325 nm, suggesting that the emission arises from the same excited state, i.e.  $S_1$  (Figure S17). However, upon gradual replacement of oxygen by sulphur (compounds ( $SO$ ) and ( $S_2$ )), a bathochromic shift of the absorption bands was observed in DMF, indicating a conjugation effect (Table 1, Figure S18–S19). This can be attributed to the lower electronegativity and higher  $\pi$ -polarizability of sulphur compared to oxygen and a weaker conjugation based on a stronger deviation from planarity. Such tilting of the structure as well as changes in the electronegativity by the bridging sulphur atoms can drastically influence the excited-state properties, such as emission profiles, lifetimes ( $\tau$ ) and  $\Phi_F$  (see Table 1 for the summarized photophysical data). For compounds  $O_2$ ,  $SO$  and  $S_2$ , a concomitant red shift with increasing sulphur content was observed in solution as well as in the solid state (powder) (Figure S17–S19 and S26), due to a drop of the energy gap mostly due to the destabilization of the HOMO. In addition, when going from compound  $O_2$  to  $SO$  and  $S_2$ , the  $\tau$  drastically increased in solution from 2 ns to 18.7 ns, although in the solid state they showed a clear attenuation tendency going from 20.8 ns to 3.7 ns (Table 1 and Figure S31–33). It is noteworthy, that  $\Phi_F$  of  $SO$  in solution (24%) and the solid state (10%) is significantly higher than  $O_2$  and  $S_2$ . These changes in the lifetimes and quantum yields can be explained by analysing the average fluorescence rate constants ( $k_f$ ) and the corresponding non-radiative deactivation rates ( $k_{nr}$ ); in general, the non-radiative processes are faster in the solid state if compared with fluid solutions, except for  $O_2$  where the  $k_{nr}$  drops in the solid while boosting  $\tau$  and  $\Phi_F$  (Table S2 and Figures S40–41).

Compounds  $O_4$ ,  $SO_3$ ,  $S_2O_2-z$ ,  $S_2O_2-e$ ,  $S_3O$  and  $S_4$  bear a pentacene-like skeleton, along with four heteroatomic substitution variations ( $X_1$ ,  $X_2$ ,  $X_3$  and  $X_4$ , Scheme 1). The absorption and excitation bands of the pentacene-like compounds (Figure S20–25) are significantly red-shifted in DMF compared to the anthracene-like cores of compounds  $O_2$ ,  $SO$  and  $S_2$  (Figure S17–

**Table 1.** Overview of the photophysical data for the reported compounds in fluid solutions and in the solid-state including wavelengths of excitation ( $\lambda_{ex}$ ) and emission ( $\lambda_{em}$ ) maxima, photoluminescence quantum yields ( $\Phi_F$ ) and amplitude-weighted average lifetimes ( $\tau_{av\_amp}$ ).

Fluid solution Compound	$\lambda_{ex}$ [a,b]	$\lambda_{em}$ [b]	$\Phi_F \pm 2\%$ [c]	$\tau_{av\_amp}/ns$ [d]	Solid state			
					$\lambda_{ex}$ [a,e]	$\lambda_{em}$ [e]	$\Phi_F \pm 2\%$ [f]	$\tau_{av\_amp}/ns$ [g]
O <sub>2</sub> [h]	325	459	3	2.05 ± 0.02	362	435	9	20.8 ± 1.0
SO	347	493	24	13.2 ± 0.1	414	468	10	5.6 ± 0.2
S <sub>2</sub>	359	558	11	18.7 ± 0.1	414	491	4	3.70 ± 0.02
O <sub>4</sub> [h]	431	481	32	10.14 ± 0.06	455	498	20	3.17 ± 0.02
SO <sub>3</sub>	435	530	33	8.11 ± 0.03	477	548	23	3.55 ± 0.02
S <sub>2</sub> O <sub>2</sub> -e	447	537	27	6.70 ± 0.03	476	593	7	1.84 ± 0.01
S <sub>2</sub> O <sub>2</sub> -z	416	574	7	4.42 ± 0.08	475	575	20	2.37 ± 0.04
S <sub>3</sub> O	443	554	19	4.48 ± 0.02	467	565	7	2.76 ± 0.02
S <sub>4</sub>	423	575	8	2.74 ± 0.01	476	546	7	1.47 ± 0.01

[a] Most bathochromic excitation maximum. [b] Dissolved in DMF. [c]  $\Phi_F$  was obtained using a calibrated integrating sphere system for optically diluted DMF solutions. [d] Amplitude-weighted average lifetime in DMF. [e] As solid using an appropriate sample holder. [f]  $\Phi_F$  of solids were obtained using a calibrated integrating sphere with a suitable sample holder. [g] Amplitude-weighted average fluorescence lifetimes in the solid state. [h] Data were partially reported in literature.<sup>[17,18a]</sup>

S19), which was attributed to the extended conjugation. Furthermore, emission profiles,  $\Phi_F$  and  $\tau$  of these compounds were investigated in depth.

Compounds O<sub>4</sub>, SO<sub>3</sub> and S<sub>2</sub>O<sub>2</sub>-e, showed a gradual red-shift of the emission peak both in solution (DMF) and in the solid state (Figure S20, S21 S25, S26 and Table 1). Structurally, compound O<sub>4</sub> contains four oxygen atoms, whereas compound SO<sub>3</sub> and S<sub>2</sub>O<sub>2</sub>-z contained one or two sulphur atoms respectively (X<sub>1</sub> and/or X<sub>2</sub> = sulphur).

Compound O<sub>4</sub> was found to be almost planar, whereas the presence of sulphur led to a puckered, non-planar geometry (see optimized structures in Figure S51–S54). This is due to the different valence angle in sulphur as compared to oxygen. The former element prefers an angle of 90° and pointing to a significant hybridization defect with a promogenic repulsion.<sup>[20]</sup>

For the oxygen atoms, the 2s orbital has only one radial node, so its radial distribution function (RDF) peaks farther away from the nucleus than in the case of 1s counterpart, whereas the 2p orbitals have no radial nodes and hence their RDF peak relatively close to the 2s function<sup>[21]</sup>. Despite their energy gaps, this formally supports potential sp hybridization and bonding angles above 100°. In sulphur, however, the 3s and 3p orbital have two and one radial nodes, respectively, and hence the 3p functions dominate the chemical bonding and angles at around 90°.

Besides their strong photoluminescence in solution, compound O<sub>4</sub>, SO<sub>3</sub> and S<sub>2</sub>O<sub>2</sub>-e also showed bright emission in the solid-state with  $\Phi_F$  reaching up to 23% and with a concomitant emission red-shift from compound O<sub>4</sub> to compound S<sub>2</sub>O<sub>2</sub>-e spanning from 498 nm to 593 nm (Table 1). Moreover, the solid-state emission profiles from O<sub>4</sub> to S<sub>2</sub>O<sub>2</sub>-e were found to be red-shifted in the solid state compared to the corresponding solutions (Figure S20, S21 and S25, Figure 1).

In contrast to the aforementioned compounds O<sub>4</sub>, SO<sub>3</sub> and S<sub>2</sub>O<sub>2</sub>-e, the compounds S<sub>3</sub>O, S<sub>2</sub>O<sub>2</sub>-z and S<sub>4</sub> contain sulphur atoms in the same bridge. We discovered only marginal changes in emission, but noted a contrary trend in the solid state, where we saw a hypsochromic shift from 575 nm for S<sub>2</sub>O<sub>2</sub>-z to 546 nm for S<sub>4</sub> with a significant decrease in  $\Phi_F$ . We assume that the presence of two sulphur atoms in the same

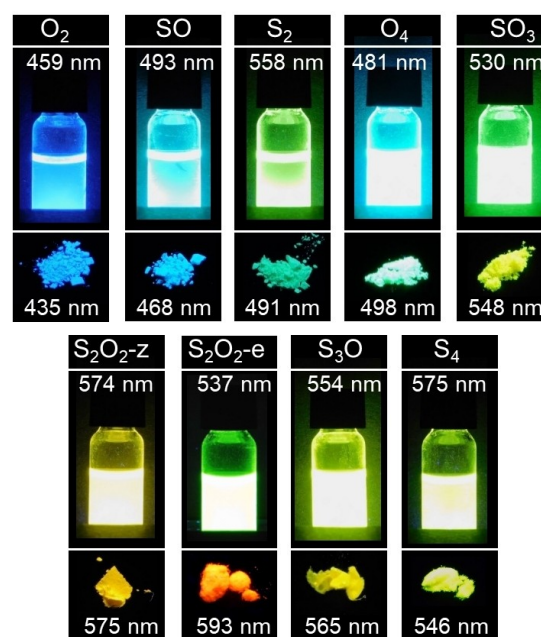


**Figure 1.** Photographs of the compounds dissolved in DMF and as powders along with the corresponding wavelength of the emission maxima.  $\lambda_{ex} = 365$  nm, concentration in DMF = 50  $\mu$ M. Photographs of compounds in DMF were performed above room temperature (60 °C) due to the low solubility in common organic solvents.

ring leads to a kink and thus to a stronger deviation from planarity than what we observed for oxygen, which favours a planar geometry (Figure S51–54). This creates a competition between the sulphur and oxygen atoms leading to distorted planar structures, which hamper the conjugation. Notably, the lifetimes of the pentacene-like compounds steadily decrease in solution with higher sulphur contents, probably because of non-radiative decay pathways which applies also for the  $\Phi_F$ , except for S<sub>3</sub>O ( $\Phi_F = 19\%$ ), whereas in the solid state the lifetimes only drop marginally (Table 1 and Figure S34–39).

In general, the presence of a polar solvent should increase the charge transfer (CT) character and decrease the energy content of the excited states.<sup>[22]</sup> However, a careful investigation of the emission maxima for all nine compounds summarized in

Table 1 revealed an inconsistent trend regarding the emission maxima in solution and in the solid state. The emission maxima of compound  $O_2$ ,  $SO$  and  $S_2$  in DMF showed a large bathochromic shift compared with their emission as pristine powders (Figure 1). However, for pentacene-like derivatives, i.e. compounds  $O_4$  to  $S_4$ , the trend mainly follows the above-mentioned expectations (except for compound  $S_2O_2-z$  and  $S_4$ ) with bathochromic shifts in the solid state with respect to solutions. Surprisingly, compound  $S_2O_2-z$  exhibits nearly identical emission profiles in solution and the solid state, whereas compound  $S_4$  displays a blue shift in the solid state if compared with the corresponding solution, which resembles the anthracene-like compounds (Figure 1). To explain this behaviour, a closer look at their structural differences is required. We found the main structural differences of the three anthracene-like and the six pentacene-like compounds to be the number and position of the bridging heteroatoms and the orientation of the nitrile groups. For the anthracene-like derivatives, the presence of the polar *ortho*-CN groups dictates the trend of the emission in solution. Because of the high polarity of DMF, the *ortho*-CN containing compounds  $O_2$ ,  $SO$  and  $S_2$  revealed a red-shifted emission compared to their solid-state forms. However, we assume that for pentacene-like compounds, the nature (sulphur/oxygen) and location of the heteroatoms mainly dictate the order of emission maxima, as both polar CN groups will nullify their polarity influence because of their oppositely located *para*- position. The influence of the nature (sulphur/oxygen) and the location of the heteroatoms can be easily compared by investigating the emission profiles. Comparison of compound  $O_4$  (four oxygens) and  $S_4$  (four sulphurs), it becomes apparent that sulphur influences the emission significantly, as compound  $S_4$  exhibits a red-shifted emission compared to  $O_4$ , both in solution and the solid state. Such control over the emission spectrum both in solution and in the solid state by simple change of the bridging heteroatom can be useful for the design of tailored materials such as gels and polymers.

The most interesting outcome was the high photoluminescence  $\Phi_F$  in solution and in the solid state (Table 1). Generally, for ACQ species, the  $\Phi_F$  in solution is prominent, while in the solid state the  $\Phi_F$  is nearly below the experimental uncertainty, which is opposed to AIE compounds where the phenomenon is exactly the opposite.  $O_4$  and  $SO_3$ , however, showed intense photoluminescence both in solution and in the solid-state. This is mainly the case because they exhibit both ACQ and AIE. In the current scenario, we have monitored the  $\Phi_F$  of all compounds in solution with a maximum value of  $\sim 33\%$ , and a solid-state  $\Phi_F$  of  $\sim 23\%$  ( $SO_3$ ) (Table 1). This observation is not only unique because of its high emission efficiency, but it also demonstrates that the materials are nearly equally emissive in solution and in the solid state, which has been rarely described. Our design approach enables the suppression of vibrational and rotational relaxation both in the solid state and in solution.

In addition to the experimental measurements, we performed quantum chemical calculations in the gas phase and in DMF using an implicit solvent model. We employed the RI-CC2/cc-pVTZ//CAM-B3LYP/6-31G\*\* level of theory and obtained absorption and emission wavelengths in qualitative agreement

with the experimental values (Table S5). The results provide an insight into the electronic structure of the ground and excited state. Furthermore, we analysed the change in the geometry in the photoexcited state. Besides the energies, we calculated the oscillator strengths that were compared to the experimental  $\Phi_F$ . The order of the  $\Phi_F$  in DMF was found to be  $SO_3$  (33%) >  $O_4$  (32%) >  $S_2O_2-e$  (27%) >  $S_3O$  (9%) >  $S_4$  (8%) >  $S_2O_2-z$  (7%) for the pentacene-like compounds and  $SO$  (24%) >  $S_2$  (11%) >  $O_2$  (3%) for the anthracene-derived samples (Table 1). The calculated oscillator strengths in DMF for the emission and absorption spectra of the pentacene-like probes follow the same trend as the  $\Phi_F$ , except for  $SO_3$  and  $S_2O_2-z$  (Table S5). For the anthracene-like species, the oscillator strength of  $O_2$  is larger than the experimental observations. The deviations might be due to the formation of aggregates or stacks in solution, due to its planar structure.

We also analysed the character of the excitation based on the changes in the electron density between the ground and excited state (Figure S54). In the anthracene-based compounds, the density moved from the  $\pi$ -type orbitals of the oxygen or sulphur atoms in the bridging position to the dicyano-phenyl core (Figure S54). These displacements indicate an intramolecular charge transfer. Therefore, these molecules should show typical charge transfer (CT) features, e.g. solvatochromism and broad emission bands devoid of vibrational progression. To support this hypothesis, compounds ( $S_2$ ) ( $O_4$ ), ( $SO_3$ ) and ( $S_2O_2-z$ ) were measured in different solvents starting from low to high polarity (Table S1 and Figure S27–S30). This influences the electronic structure and the charge distribution of the compounds, and consequently, their ground and excited state. The resulting solvatochromic effect was detectable with the naked eye (Figure S27–S30). The pentacene-based compounds showed similar charge transfer character, where the electron density was moving from the bridging group atoms to the dicyano groups in the center of the compounds (Figure S54).

The displacement of the electron density caused significant alterations in the excited-state geometry. The anthracene-based compounds became fully planar in the excited state (Figure S54). For the pentacene-based compounds, we could observe a planarization, too; however the extent of the planarization depended on the number of oxygen and sulphur atoms in the bridging positions (see optimized structures of the anthracene and pentacene-like compounds provided in Figure S50–53). In cases with none, one or two sulphur atoms, the excited-state geometry was planar, while for three or four sulphur atoms the compounds became noticeably more planar compared to the ground state geometry, but remained kinked. These changes in the geometry were also reflected in the correlation between the excited-state reorganisation energy ( $\lambda_{S1}$ ) and the root-mean-square deviation (RMSD) between ground-state and excited-state geometry (Figure S55, Tab S6). There, an increase in RMSD corresponded to an enhancement in  $\lambda_{S1}$ . The exceptions were the *Z* conformations of the pentacene-like compounds, where the associated increase in  $\lambda_{S1}$  was smaller than for the rest.

The possible dual conformation (*E* and *Z*) of compound  $S_3O$ ,  $S_4$  to  $S_2O_2-e$  suggested by theoretical calculations inspired us to

check the influence of polymorphism on the photophysical properties (Figure S52 and S53). Polymorphism is a highly interesting phenomenon to investigate, e.g., the influence of molecular packing on the photophysical properties without changing the composition of the sample. We were able to grow single crystals of compound  $S_2O_2-e$  ( $X_1 = X_4 = \text{sulphur}$  and  $X_2 = X_3 = \text{oxygen}$ ), which were analyzed by X-ray diffractometry. Furthermore,  $S_2O_2-e$  was of special interest due to its extreme bathochromic emission shift between solution and solid state. Hence, we assumed a larger influence of the crystal packing on the emission profile. Crystals suitable for X-ray diffraction were obtained by very slow evaporation of a DMF solution (3 months). Two different sets of crystals were found to grow in the same vial – plate-like yellow  $S_2O_2-e$  (A) and needle-like red  $S_2O_2-e$  (B) (Figure 2B–D). We carefully isolated them and conducted optical measurements and crystal packing determination. The emission spectra revealed that the two polymorphs of  $S_2O_2-e$  featured different emission profiles (Figure 2A) most likely due to their different packing in the crystal and a different microenvironmental dielectric constant. The red and the yellow polymorphs showed emission maxima at  $\sim 572$  nm and 540 nm, respectively. These kind of organic luminescence materials that exhibit distinct luminescence colour in the solid state without changing the chemical structure of their component molecules have attracted increasing interest in recent years.<sup>[23]</sup> For example, Wang and co-workers prepared stimuli responsive reversible colour switching crystal polymorphs using fluorenone derivatives.<sup>[24]</sup> In our case, we expected that the colour differences mainly arose from the differences in the microenvironment and we therefore investigated their packing in the crystal in detail.

Both polymorphs were packed in the centrosymmetric ( $P2_1/c$ ) space group within a monoclinic system and possessed a

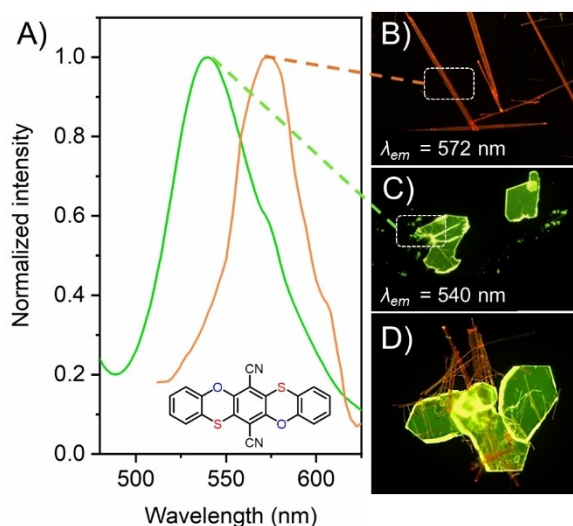


**Figure 2.** A) Photoluminescence spectra of the two polymorphs as single crystals. B) Fluorescence microscopy image of the red polymorph of compound  $S_2O_2-e$  (B). C) Fluorescence microscopy image of the yellow polymorph of compound  $S_2O_2-e$  (A). D) Fluorescence microscopy image of both polymorphs grown together from a saturated DMF solution. ( $\lambda_{ex} = 365$  nm).

versatile packing pattern (Figure S40–47). We found them to deviate from planarity because of the bridging heteroatoms (oxygen and sulphur), which assisted the suppression of ACQ phenomena. For example, the torsion angles of the yellow polymorph  $S_2O_2-e$  (A) were found to be C1–C2–O1–C10  $157.7^\circ$ ; C1–C3\*–S1\*–C5\*  $163.0^\circ$  and for the red polymorph ( $S_2O_2-e$  (B)) C1–C2–O1–C10  $153.7^\circ$ ; C1–C3\*–S1\*–C5\*  $165.0^\circ$  (Figure 3, S42–49).

Most interestingly, the differences between the packing pattern of  $S_2O_2-e$  (A) and  $S_2O_2-e$  (B) were the appearance of an orthogonal arrangement for the yellow polymorph  $S_2O_2-e$  (A) and slipped parallel stacking for the red polymorph  $S_2O_2-e$  (B) (Figure 3). For the yellow polymorph, the orthogonal packing was formed via multiple  $\pi \cdots \pi$  interactions between the molecules with an orthogonal orientation, supported by numerous O  $\cdots \pi$  interactions (O1  $\cdots$  C4  $3.091$  Å) involving the bridging oxygen atom and one adjacent CN group (Figure 3).

The sulphur atom is involved in the formation of weak C–H  $\cdots$  S interactions (C7–H7  $\cdots$  S1  $3.946(1)$  Å;  $154.8^\circ$ , Tab S3). In contrast, the packing diagram of the red-emissive  $S_2O_2-e$  (B) presented the formation of linear chains involving S  $\cdots \pi$  interactions (Cg1  $\cdots$  S1  $3.492$  Å and Cg2  $\cdots$  S1  $3.464$  Å, Table S4). Notably, in the red polymorph  $S_2O_2-e$  (B), with a parallel orientation,  $\pi \cdots \pi$  contacts are more likely to occur resulting in a red-shifted emission, which is not the case in  $S_2O_2-e$  (A) (a quantitative analysis of non-covalent interaction is presented *vide infra*, see also ESI Figures S56–60). Another remarkable observation for these two polymorphs was the presence of numerous noncovalent interactions leading to the specific packing differences in the crystal (Figure 3). These noncovalent

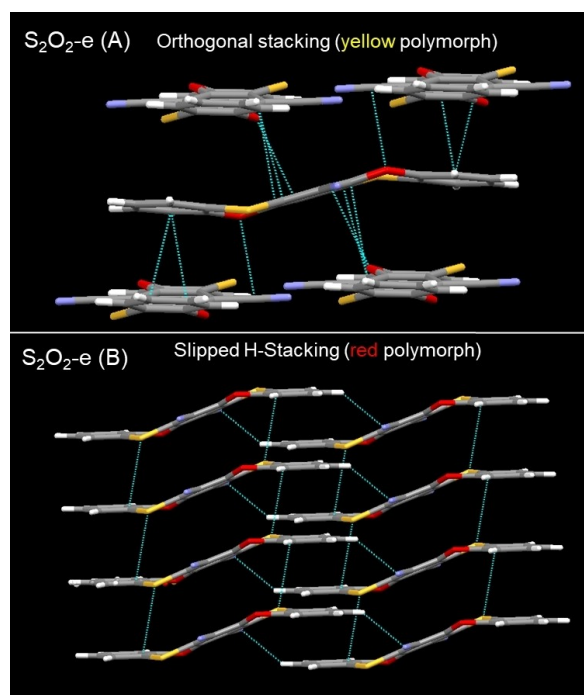


**Figure 3.** Molecular structures and packing of compounds  $S_2O_2-e$  (A) (yellow polymorph, CCDC 1913837) and  $S_2O_2-e$  (B) (red polymorph, CCDC 1913838) as obtained by X-ray diffractometric analyses.

interactions are noteworthy, as they determined the photoluminescence of the crystals in the neat solid state. Hence, we analysed noncovalent interactions using the *Hirshfeld* surface analysis (Crystal Explorer).<sup>[25]</sup> This kind of surface analysis is able to provide quantitative values of associated noncovalent interactions within the crystal, employing *di* (distance internal) and *de* (distance external) with the formation of a *d*-norm surface (Figure S57 and S59). After careful surface analysis, we monitored numerous interactions that were present within the crystal packing (Figures S56–S60). However, to make our discussion concise, we will only focus on the main interactions that dictated the solid-state optical properties, i.e., C–H... $\pi$  (indicated by C–H),  $\pi$ ... $\pi$  (indicated by C–C), S... $\pi$  (indicated as S–S) and *Van der Waals* interactions (indicated by H–H). Polymorph **S<sub>2</sub>O<sub>2</sub>-e (B)** was found to exhibit a slightly higher percentage of C–C and S–C interactions than **S<sub>2</sub>O<sub>2</sub>-e (A)**, indicating a higher contribution of  $\pi$ -contacts, which resulted in a red shifted emission (Figure 2B). Polymorph **S<sub>2</sub>O<sub>2</sub>-e (A)** revealed a brighter, blue shifted emission, as observable under the fluorescence microscope (Figure 2C), which was attributed to a higher accumulated percentage of C–H... $\pi$  interactions in **S<sub>2</sub>O<sub>2</sub>-e (A)** compared to **S<sub>2</sub>O<sub>2</sub>-e (B)** (Figure S60). The contribution of *Van der Waals* interactions is almost equal for both polymorphs. Owing to the low energy (~0.4–4 kJ/mol) of *Van der Waals* interactions, we assume only a negligible contribution to the optical properties in the solid state.

## Conclusion

In conclusion, we have implemented a novel concept to design highly luminescent probes able to emit in solution and the solid state, based on bridged oxo- and/or thioethers. The designed molecules showed intense emission in fluid solution and in the solid state with  $\Phi_F$  of up to 33% and 23%, respectively. We rationalized their properties using quantum chemical calculations and different photophysical characterization methods. Moreover, the polymorphism of compound **S<sub>2</sub>O<sub>2</sub>-e** was assessed using X-ray crystallography as well as a supporting *Hirshfeld* surface analysis. The results showed a potential design strategy for the development of highly efficient luminophores emitting both in solution and in the solid state.

## Experimental Section

The synthetic procedures as well as analytical details for the compounds used in this study can be found in the electronic supplementary information.

### General

All chemicals were purchased from Sigma Aldrich or from TCI Chemicals and used without further purification. All reactions were performed using dried solvents. Reaction progress was monitored by thin-layer chromatography (TLC), (0.2 mm Macherey-Nagel ALU-GRAM precoated silica gel aluminum sheets). Spots on the TLC plates were visualized by treatment with basic KMnO<sub>4</sub> solution or

by an UV-handlamp (254 and 365 nm). Column chromatography was performed using SiO<sub>2</sub> 60 (0.063–0.2 mm, Merck). K<sub>2</sub>CO<sub>3</sub> was freshly ground and dried at 90 °C. To remove water, a freeze dryer was used (Alpha 1-4 LD plus, Martin Christ Gefriertrocknungsanlagen GmbH). NMR spectra were recorded on a Bruker DMX 300 spectrometer [<sup>1</sup>H: 300.16 MHz, <sup>13</sup>C: 75.47 MHz] or DMX 600 [<sup>1</sup>H: 600.16 MHz, <sup>13</sup>C: 151.47 MHz]. The chemical shifts are referenced relative to the residual proton signals of the solvents. Coupling constants (*J*) are reported in Hertz (Hz). High resolution mass spectra were measured on a Bruker maXis 4G UHR-TOF or on a LTQ Orbitrap LTQ XL (Thermo-Fisher Scientific, Bremen). The infrared spectra were recorded using a VARIAN 3100 FT-IR (excalibur series).

### Single crystal X-ray analysis

Data sets for compound **S<sub>2</sub>O<sub>2</sub>-e (A)** were collected with a Bruker D8 Venture CMOS diffractometer. Programs used: data collection: APEX3V2016.1-0,<sup>[26]</sup> cell refinement: SAINT V8.37 A,<sup>[26]</sup> data reduction: SAINT V8.37A,<sup>[26]</sup> absorption correction, SADABS V2014/7,<sup>[26]</sup> structure solution SHELXT-2015,<sup>[27a]</sup> structure refinement SHELXL-2015.<sup>[27b]</sup> For compound **S<sub>2</sub>O<sub>2</sub>-e (B)** data sets were collected with a Nonius Kappa CCD diffractometer. Programs used: data collection, COLLECT;<sup>[28]</sup> data reduction Denzo-SMN,<sup>[29]</sup> absorption correction, Denzo,<sup>[30]</sup> structure solution SHELXT-2015,<sup>[27a]</sup> structure refinement SHELXL-2015.<sup>[27b]</sup> Further information can be found in the electronic supplementary information.

## Acknowledgements

The authors acknowledge the Deutsche Forschungsgemeinschaft (Grant: VO 2383/1-1 to JV) and Mercator Fellowship (Grant: SFB 1078 to IS). We furthermore thank the Alexander von Humboldt Foundation (Postdoctoral fellowship to IM), the Cells in Motion Cluster of Excellence DFG EXC1003 and DFG/Land NRW: INST 211/915-1 FUGG (funding for CAS), the Minerva Foundation (Postdoctoral fellowship to SA) and the European Research Council (ERC) under the European Union's Horizon 2020 research and innovation programme (Grant Agreement No. 678169, ERC Starting Grant "PhotoMutant", funding to IS). Harini Hemesh, Darío González Abradelo and Jan Balszuweit are acknowledged for support during the synthesis and the photophysical characterisation. Open access funding enabled and organized by Projekt DEAL via the University of Duisburg-Essen. Open access funding enabled and organized by Projekt DEAL.

## Conflict of Interest

The authors declare no conflict of interest.

**Keywords:** Luminophores · Solution and solid-state emitter (SSSE) · Bridged ethers · Aromatics

- [1] L. Le Bras, K. Chaitou, S. Aloise, C. Adamo, A. Perrier, *Phys. Chem. Chem. Phys.* **2018**, *21*, 46–56.
- [2] F. Würthner, *Angew. Chem. Int. Ed.* **2020**, *59*, 14192–14196; *Angew. Chem.* **2020**, *132*, 14296–14301.
- [3] a) G. Oster, Y. Nishijima, *J. Am. Chem. Soc.* **1956**, *78*, 1581–1584; b) G. Scheibe, *Angew. Chem.* **1936**, 563; c) G. C. Schmidt, *Ann. Phys.* **1921**, *370*, 247–256, <https://doi.org/10.1002/andp.19213701105>.

- [4] a) L. G. Lee, C.-H. Chen, L. A. Chiu, *Cytometry* **1986**, *7*, 508–517; b) J. Nygren, N. Svanvik, M. Kubista, *Biopolymers* **1998**, *46*, 39–51.
- [5] J. Luo, Z. Xie, J. W. Y. Lam, L. Cheng, H. Chen, C. Qiu, H. S. Kwok, X. Zhan, Y. Liu, D. Zhu, B. Z. Tang, *Chem. Commun.* **2001**, 1740–1741.
- [6] a) Y. C. Chen, J. W. Y. Lam, R. T. K. Kwok, B. Liu, B. Z. Tang, *Mater. Horiz.* **2019**, *6*, 428–433; b) M. Hayduk, S. Riebe, J. Voskuhl, *Chem. Eur. J.* **2018**, *24*, 12221–12230; c) J. Mei, N. L. Leung, R. T. Kwok, J. W. Lam, B. Z. Tang, *Chem. Rev.* **2015**, *115*, 11718–11940.
- [7] a) S. Riebe, C. Vallet, F. van der Vight, D. Gonzalez-Abradelo, C. Wolper, C. A. Strassert, G. Jansen, S. Knauer, J. Voskuhl, *Chem. Eur. J.* **2017**, *23*, 13660–13668; b) S. Feng, S. Gong, G. Feng, *Chem. Commun.* **2020**, *56*, 2511–2513.
- [8] S. Thulaseedharan Nair Sailaja, I. Maisuls, J. Kosters, A. Hepp, A. Faust, J. Voskuhl, C. A. Strassert, *Beilstein J. Org. Chem.* **2020**, *16*, 2960–2970.
- [9] G. Chen, W. Li, T. Zhou, Q. Peng, D. Zhai, H. Li, W. Z. Yuan, Y. Zhang, B. Z. Tang, *Chem. Sci.* **2015**, *27*, 4496–4501.
- [10] J. N. Zhang, H. Kang, N. Li, S. M. Zhou, H. M. Sun, S. W. Yin, N. Zhao, B. Z. Tang, *Chem. Sci.* **2017**, *8*, 577–582.
- [11] A. Raghuvanshi, A. K. Jha, A. Sharma, S. Umar, S. Mishra, R. Kant, A. Goel, *Chem. Eur. J.* **2017**, *23*, 4527–4531.
- [12] J. Wang, Z. Liu, S. Yang, Y. Lin, Z. Lin, Q. Ling, *Chem. Eur. J.* **2018**, *24*, 322–326.
- [13] M. Huang, J. Zhou, K. Xu, X. Zhu, Y. Wan, *Dyes Pigm.* **2019**, *160*, 839–847.
- [14] M. Huang, R. Yu, K. Xu, S. Ye, S. Kuang, X. Zhu, Y. Wan, *Chem. Sci.* **2016**, *7*, 4485–4491.
- [15] J. Zhou, M. Huang, X. Zhu, Y. Wan, *Chin. Chem. Lett.* **2021**, *32*, 445–448.
- [16] E. J. Wang, J. W. Y. Lam, R. R. Hu, C. Zhang, Y. S. Zhao, B. Tang, *J. Mater. Chem. C* **2014**, *2*, 1801–1807.
- [17] S. Banerjee, A. Chattopadhyay, A. Banerjee, M. Haridas, P. Saini, M. Das, M. S. Majik, Y. K. Maurya, *Bioorg. Med. Chem. Lett.* **2015**, *25*, 753–757.
- [18] a) L. K. Hiscock, C. Yao, W. G. Skene, L. N. Dawe, K. E. Maly, *J. Org. Chem.* **2019**, *84*, 15530–15537; b) B. Zhang, M. Wei, H. Mao, X. Pei, S. A. Alshmiri, J. A. Reimer, O. M. Yaghi, *J. Am. Chem. Soc.* **2018**, *140*, 12715–12719.
- [19] W. Xi, J. Yu, M. Wei, Q. Qiu, P. Xu, Z. Qian, H. Feng, *Chem. Eur. J.* **2020**, *26*, 3733–3737.
- [20] W. Kutzelnigg, *Angew. Chem. Int. Ed.* **1984**, *23*, 272–295; *Angew. Chem.* **1984**, *96*, 262–286.
- [21] P. P. Power, *Organometallics* **2020**, *39*, 4127–4138.
- [22] a) B. Roy, M. C. Reddy, P. Hazra, *Chem. Sci.* **2018**, *9*, 3592–3606; b) B. Roy, M. C. Reddy, G. P. Jose, F. C. Niemeyer, J. Voskuhl, P. Hazra, *J. Phys. Chem. Lett.* **2021**, *12*, 1162–1168.
- [23] S. M. Pratik, A. Nijamudheen, S. Bhattacharya, A. Datta, *Chem. Eur. J.* **2014**, *20*, 3218–3224.
- [24] X. Du, F. Xu, M.-S. Yuan, P. Xue, L. Zhao, D.-E. Wang, W. Wang, Q. Tu, S.-W. Chen, J. Wang, *J. Mater. Chem. C* **2016**, *4*, 8724–8730.
- [25] a) M. A. Spackman, D. Jayatilaka, *CrystEngComm* **2009**, *11*, 19–32; b) M. A. Spackman, J. J. McKinnon, *CrystEngComm* **2002**, *4*, 378–392.
- [26] Bruker AXS (2016) - APEX3 (2016), SAINT (2015) and SADABS (2015), Bruker AXS Inc., Madison, Wisconsin, USA.
- [27] a) G. M. Sheldrick, *Acta Crystallogr. Sect. A* **2015**, *71*, 3–8; b) G. M. Sheldrick, *Acta Crystallogr. Sect. C* **2015**, *71*, 3–8.
- [28] R. W. W. Hooft, B. V. Nonius, COLLECT, Program for Collecting Data on CCD Area Detectors, **1998**, Delft, The Netherlands.
- [29] Z. Otwinowski, W. Minor, in *Methods Enzymol.*, Vol. 276, Academic Press, **1997**, pp. 307–326.
- [30] Z. Otwinowski, D. Borek, W. Majewski, W. Minor, *Acta Crystallogr. Sect. A* **2003**, *59*, 228–234.

---

Manuscript received: May 7, 2021  
 Revised manuscript received: June 21, 2021  
 Accepted manuscript online: June 22, 2021  
 Version of record online: July 6, 2021